# CONTROLLING HIDDEN DYNAMICS AND MULTI-STABILITY OF A CLASS OF TWO-DIMENSIONAL MAPS VIA LINEAR AUGMENTATION

LIPING ZHANG
*Faculty of Civil Engineering and Mechanics,*
*Jiangsu University, Zhenjiang 212013, P. R. China*
*School of Mathematics and Statistics, Yancheng Teachers University,*
*Yancheng 224002, P.R. China*
*yctczlp@126.com*

HAIBO JIANG*
*School of Mathematics and Statistics, Yancheng Teachers University,*
*Yancheng 224002, P.R. China*
*yctcjhb@126.com*

YANG LIU
*College of Engineering, Mathematics and Physical Sciences, University of Exeter,*
*Harrison Building, North Park Road, Exeter, EX4 4QF, UK*
*y.liu2@exeter.ac.uk*

ZHOUCHAO WEI
*School of Mathematics and Physics, China University of Geosciences,*
*Wuhan 430074, P.R. China*
*weizhouchao@163.com*

QINSHENG BI
*Faculty of Civil Engineering and Mechanics,*
*Jiangsu University, Zhenjiang 212013, P. R. China*
*qbi@ujs.edu.cn*

Received (to be inserted by publisher)

This paper reports the complex dynamics of a class of two-dimensional maps containing hidden attractors via linear augmentation. Firstly, the method of linear augmentation for continuous dynamical systems is generalised to discrete dynamical systems. Then three cases of a class of two-dimensional maps that exhibit hidden dynamics, the maps with no fixed point and the maps with one stable fixed point, are studied. Our numerical simulations show the effectiveness of the linear augmentation method. As the coupling strength of the controller increases or decreases, hidden attractor can be annihilated or altered to be self-excited, and multi-stability of the map can be controlled to bistable or monostable.

*Keywords*: Chaotic map; Linear augmentation; Bifurcation analysis; Hidden attractor; Control of multi-stability.

*Author for correspondence.

## 1. Introduction

Since the concept of hidden dynamics for dynamical systems was proposed [Leonov & Kuznetsov, 2013], the complexity of hidden attractors has been studied extensively [Dudkowski *et al.*, 2016a]. Special continuous systems which contain hidden attractors have been investigated by many researchers, e.g. the continuous systems with no equilibria [Wei, 2011; Jafari *et al.*, 2013; Wang *et al.*, 2016; Dantsev, 2018; Zhan *et al.*, 2018] and the continuous systems with only stable equilibria [Wang & Chen, 2012; Molate *et al.*, 2013; Wei & Zhang, 2014; Lai *et al.*, 2018]. In particular, the continuous systems with different types of infinite equilibria have been studied, such as the ones with any number of equilibria [Wang & Chen, 2013], with a line of equilibria [Jafari & Sprott, 2013; Li *et al.*, 2014b; Zhou & Yang, 2014; Li *et al.*, 2014a], with the curves of equilibria [Chen & Yang, 2015; Barati *et al.*, 2016; Gotthans *et al.*, 2016; Pham *et al.*, 2016; Wang *et al.*, 2017], with the planes of equilibria [Jafari *et al.*, 2016a; Bao *et al.*, 2017], and with the surfaces of equilibria [Jafari *et al.*, 2016b; Singh *et al.*, 2018]. On the other hand, several special maps which have hidden attractors have also been studied, e.g. the maps with no fixed point [Jafari *et al.*, 2016c; Jiang *et al.*, 2016a,b; Panahi *et al.*, 2018; Wang *et al.*, 2018], the maps with only stable fixed points [Jiang *et al.*, 2016a,b], and the maps with different types of infinite fixed points [Chen *et al.*, 2017; Liu *et al.*, 2017; Jiang *et al.*, 2019; Bao *et al.*, 2020; Zhang *et al.*, 2020]. In practice, hidden attractors have been found in real-world applications, such as electrical circuits [Leonov & Kuznetsov, 2013; Dudkowski *et al.*, 2016a; Pham *et al.*, 2017], downhole drilling [Leonov & Kuznetsov, 2013; Dudkowski *et al.*, 2016a; Leonov *et al.*, 2016], and vibration-driven robots [Liu & Páez Chávez, 2017b]. In these systems, hidden dynamics can be utilised for control purposes if the hidden attractor is more efficient in the point of view of energy consumption [Liu & Páez Chávez, 2017b], while it could also cause catastrophic failures if the hidden dynamics is harmful to the system, e.g. the cause of severe stick-slip oscillations in downhole drilling [Liu *et al.*, 2019]. Therefore, better understanding and control of hidden attractors become crucial.

As explained, since the nonlinear systems with hidden attractors can produce many unexpected responses, such as the stick-slip motion in downhole drilling [Liu *et al.*, 2020], controlling hidden dynamics has received great attention from the research community. Many control methods have been studied, such as passive control [Sambas *et al.*, 2019], adaptive control [Wei *et al.*, 2014; Jahanshahi *et al.*, 2019], adaptive backstepping control [Vaidyanathan *et al.*, 2018], adaptive sliding mode control [Mobayen, 2018; Wei *et al.*, 2018], and delayed feedback control [Feng & Wei, 2015; Wang *et al.*, 2015]. In [Wei *et al.*, 2014], an adaptive control law was designed to stabilise the extended Sprott E system with hidden attractors. In [Feng & Wei, 2015], a delayed feedback controller was used to control the bifurcation of a generalized Sprott B system with hidden attractors. Wang et al. [Wang *et al.*, 2015] developed a delayed feedback control scheme for a class of 3D jerk systems with only one stable equilibria, and analysed the Hopf bifurcation observed in the controlled system. In [Vaidyanathan *et al.*, 2018], Vaidyanathan et al. investigated the adaptive backstepping control of a 4-D chaotic hyperjerk system containing a hidden chaotic attractor. In [Mobayen, 2018], a novel adaptive sliding mode control technique was proposed for stabilising the perturbed Chameleon hidden chaotic flows. Wei et al. [Wei *et al.*, 2018] studied the control problem of hidden chaos in a self-exciting homopolar disc dynamo by using a nonlinear feedback control, a sliding mode control, and the combination of both controllers. Recently, an adaptive radial-basis function neural network-based control method was proposed to stabilise a class of four-dimensional chaotic system with hidden attractors [Jahanshahi *et al.*, 2019]. Sambas et al. [Sambas *et al.*, 2019] studied a passive control method for stabilising a new chaotic system with line equilibrium which displays hidden chaotic attractors.

More recently, linear augmentation has been widely adopted for control purposes. In [Sharma *et al.*, 2011], Sharma et al. proposed a general linear augmentation control strategy to stabilise the fixed points of nonlinear oscillators. Then they used the method to drive a bistable system to a desired attractor by annihilating the other one [Sharma *et al.*, 2013]. In [Sharma *et al.*, 2014], they studied a simple scheme of linear augmentation for controlling the dynamical behaviour of a drive-response system through either suppression of oscillations or annihilation of one of its coexisting attractors. Karnatak [Karnatak, 2015] studied the stabilisation of desired stationary solutions of oscillatory systems using linear augmentation from a more general sense. In the paper, some simple examples were given to prove the effectiveness of the proposed scheme, and a careful analysis for the potential pitfalls associated with the scheme was presented.

Liu and Páez Chávez [Liu & Páez Chávez, 2017a] studied the control of coexisting attractors in an impacting system via a new control law based on linear augmentation. It has found that the proposed control law can effectively switch between coexisting attractors without altering the system's main parameters and avoiding grazing-induced chaotic responses. In [Thounaojam & Shrimali, 2018], the authors studied the phase-flip in relay oscillators by considering both time delay and conjugate couplings, and also implemented linear augmentation to control the dynamics of the relay oscillators. In [Fonzin Fozin *et al.*, 2019a,b,c; Tabekoueng Njitacke et al., 2020], Kengne's team investigated the control of multi-stability of several complex systems by using linear augmentation.

In the present work, we aim to control hidden dynamics and multi-stability of a class of new two-dimensional maps which have been found recently by Jiang et al. [Jiang *et al.*, 2016a]. The main contributions of this paper are: (1) the generalisation of linear augmentation from continuous dynamical systems to nonlinear maps; (2) the first time that linear augmentation is used to control the hidden dynamics and multi-stability of nonlinear maps; (3) a new method to show the evolution and categories of attractors in nonlinear maps. Furthermore, the proposed method is easy to be implemented and does not require the change of systems parameters of the original map. The method to display the hidden and self-excited attractors of nonlinear maps using bifurcation diagrams and the sampling method are general and effective, which can be used for studying other maps. The rest of this paper is organized as follows. In Section 2, the method of linear augmentation for controlling general maps is given, and the mathematical model of the augmented map which is a class of two-dimensional maps coupled with a linear map is studied. In addition, the existence and stability of fixed points of the augmented map are studied. In Section 3 and 4, controlling the hidden dynamics and multi-stability of the two-dimensional maps without fixed points and with only one stable fixed point are studied. Finally, some conclusions are drawn in Section 5.

## 2. Problem statement

Consider a class of nonlinear maps

$$X_{k+1} = F(X_k), \tag{1}$$

where $F$ denotes a nonlinear function, $X \in R^n$ represents the state of the nonlinear maps, and $k$ is the step of the nonlinear maps.

Inspired by the idea of linear augmentation for continuous dynamical systems, we propose the method of linear augmentation for discrete dynamical systems as follows. The equation of the nonlinear maps via linear augmentation is given as

$$\begin{cases} X_{k+1} = F(X_k) + \varepsilon U_k, \\ U_{k+1} = \delta U_k - \varepsilon(X_k - B), \end{cases} \tag{2}$$

where $\varepsilon$ describes the coupling strength between the nonlinear and the linear maps, $U \in R^m$ is the state of the linear coupling map, $U_{k+1} = \delta U_k$, where $\delta$ is the decay parameter. The linear map approaches to zero if the decay parameter $|\delta| < 1$ and the coupling with the nonlinear map $\varepsilon(X_k - B) = 0$. Here, $B$ is another coupling parameter of the augmented map which can be used to locate the position of fixed points.

To study the effectiveness of the proposed control method for nonlinear maps, the following definitions of hidden and self-excited attractors are recalled.

**Definition 2.1.** [Leonov *et al.*, 2016] An attractor is called a hidden attractor if its basin of attraction does not intersect with small neighborhoods of the equilibria (fixed points) of the system (map), otherwise it is called a self-excited attractor.

**Remark 2.1** In some special cases, e.g. [Jafari *et al.*, 2016c; Jiang *et al.*, 2016a,b; Panahi *et al.*, 2018; Wang *et al.*, 2018], we can distinguish between hidden and self-excited attractors directly by using Definition 2.1. For example, there is no fixed point or a single stable fixed point in the map, so the existing attractors except the fixed points are all hidden. One can also observe attractor's basin of attraction for which is hidden if it does not contain any fixed points, otherwise is self-excited. The shortcoming of this method is that it is not applicable to high-dimensional maps since their basins of attraction are difficult

to be visualised. If fixed points exist, we can use the sampling method [Dudkowski *et al.*, 2016b; Brzeski & Perlikowski, 2019; Faghani *et al.*, 2020] to determine whether the attractor is hidden or self-excited. This can be done by taking many initial points from the small neighbours of these fixed points randomly. If all these initial points do not tend to one attractor, this attractor is hidden, otherwise it is self-excited.

In [Jiang *et al.*, 2016a], a class of new two-dimensional maps was presented to show three cases of existence of hidden attractors. The difference equations of these two-dimensional maps can be written as

$$\begin{cases} x_{k+1} = y_k, \\ y_{k+1} = a_1 x_k + a_2 y_k + a_3 x_k^2 + a_4 y_k^2 + a_5 x_k y_k + a_6. \end{cases} \tag{3}$$

where $a_i \in R$, $i = 1, 2, \cdots, 6$ are real coefficients, $(x_k, y_k)$, $k \in N$, are the states of the map, $(x_0, y_0)$ is the initial value of the map.

The fixed point of map (3) can be obtained by solving the following equation

$$\begin{cases} x = y, \\ y = a_1 x + a_2 y + a_3 x^2 + a_4 y^2 + a_5 xy + a_6. \end{cases} \tag{4}$$

Then the problem of finding the fixed point can be converted to solve the following equation with respect to $y$,

$$(a_3 + a_4 + a_5)y^2 + (a_1 + a_2 - 1)y + a_6 = 0. \tag{5}$$

If $a_3 + a_4 + a_5 \neq 0$, $\Delta = (a_1 + a_2 - 1)^2 - 4(a_3 + a_4 + a_5)a_6$ is denoted as the discriminant of Eq. (5).

By coupling a linear augmentation to the second equation of map (3), we obtain the following augmented map,

$$\begin{cases} x_{k+1} = y_k, \\ y_{k+1} = a_1 x_k + a_2 y_k + a_3 x_k^2 + a_4 y_k^2 + a_5 x_k y_k + a_6 + \varepsilon u_k, \\ u_{k+1} = \delta u_k - \varepsilon(y_k - b), \end{cases} \tag{6}$$

where $\varepsilon$, $\delta$ and $b$ are the real parameters of the linear augmentation.

The fixed point of the augmented map (6) can be obtained by solving the following equation

$$\begin{cases} x = y, \\ y = a_1 x + a_2 y + a_3 x^2 + a_4 y^2 + a_5 xy + a_6 + \varepsilon u, \\ u = \delta u - \varepsilon(y - b). \end{cases} \tag{7}$$

Likewise, the problem of finding the fixed points of the augmented map (6) can be converted to solve the following equation with respect to $y$,

$$(a_3 + a_4 + a_5)y^2 + (a_1 + a_2 - 1 - \frac{\varepsilon^2}{1-\delta})y + (a_6 + \frac{\varepsilon^2 b}{1-\delta}) = 0. \tag{8}$$

If $a_3 + a_4 + a_5 \neq 0$, $\bar{\Delta} = (a_1 + a_2 - 1 - \frac{\varepsilon^2}{1-\delta})^2 - 4(a_3 + a_4 + a_5)(a_6 + \frac{\varepsilon^2 b}{1-\delta})$ can be denoted as the discriminant of Eq. (8).

Assume that the augmented map (6) has a fixed point $(x^*, y^*, u^*)$. The Jacobian matrix of the augmented map at this fixed point can be written as

$$J = \begin{bmatrix} 0 & 1 & 0 \\ a_1 + 2a_3 x^* + a_5 y^* & a_2 + 2a_4 y^* + a_5 x^* & \varepsilon \\ 0 & -\varepsilon & \delta \end{bmatrix}, \tag{9}$$

and the corresponding characteristic equation of the Jacobian matrix is given as

$$\det(\lambda I - J) = \lambda^3 + p\lambda^2 + q\lambda + r = 0, \tag{10}$$

where $p = -\mathrm{tr}(J) = -(a_2 + 2a_4 y^* + a_5 x^* + \delta)$, $q = \varepsilon^2 - a_1 - 2a_3 x^* - a_5 y^* + a_2\delta + 2a_4\delta y^* + a_5\delta x^*$, $r = -\det(J) = \delta(a_1 + 2a_3 x^* + a_5 y^*)$, $\mathrm{tr}(J) = a_2 + 2a_4 y^* + a_5 x^* + \delta$ is the trace of the Jacobian matrix and $\det(J) = -\delta(a_1 + 2a_3 x^* + a_5 y^*)$ is the determinant of the Jacobian matrix.

It should be noted that the fixed point $(x^*, y^*, z^*)$ is stable if the roots $\lambda_1, \lambda_2, \lambda_3$ of the characteristic equation (10) satisfy $|\lambda_{1,2,3}| < 1$, where $|\cdot|$ denotes the modulus of a complex number. If three eigenvalues

of the Jacobian matrix lie inside the unit circle, the fixed point is stable. If one of them lies outside the unit circle, the fixed point is unstable. It is well known that there are only three codimension-1 bifurcations of fixed points in nonlinear maps [Kuznetsov, 1998]. If one of the three eigenvalues is $+1$, saddle-node bifurcation will occur. If one of the three eigenvalues is $-1$, period-doubling bifurcation may appear. Let $j$ be the imaginary unit satisfying $j^2 = -1$. If two of the three eigenvalues are $e^{\pm j\theta}$, $0 < \theta < \pi$, i.e., there is a pair of conjugate complex eigenvalues and the modulus of the conjugate complex eigenvalues is 1, Neimark-Sacker bifurcation may take place.

## 3. Controlling two-dimensional maps with no fixed point via linear augmentation

According to [Jiang *et al.*, 2016a], when Eq. (5) has no solution, map (3) has no fixed point. Next, we will show the effectiveness of the linear augmentation by considering two cases, no fixed point I (NFI) and no fixed point II (NFII) as follows.

### 3.1. *No Fixed Point I*

If $a_3 + a_4 + a_5 = 0$, $a_1 + a_2 - 1 = 0$ and $a_6 \neq 0$, Eq. (5) has no solution, and map (3) has no fixed point. In this case, for any existing attractors, they must be hidden as their basins of attraction do not contain any fixed point. We can choose $\varepsilon$, $\delta$ and $b$ such that $\frac{\varepsilon^2}{1-\delta} \neq 0$ and $a_6 + \frac{\varepsilon^2 b}{1-\delta} \neq 0$, and then Eq. (7) has a single solution. Thus, the augmented map (6) has a single fixed point.

For the first example of NFI, we choose $a_1 = 1$, $a_2 = 0$, $a_3 = 0.51$ , $a_4 = 1$, $a_5 = -1.51$, and $a_6 = -0.74$, and the equations of the map ($\text{NFI}_c$ in [Jiang *et al.*, 2016a]) can be written as

$$\begin{cases} x_{k+1} = y_k, \\ y_{k+1} = x_k + 0.51x_k^2 + y_k^2 - 1.51x_k y_k - 0.74. \end{cases} \tag{11}$$

Based on [Jiang *et al.*, 2016a], map (11) has a single chaotic attractor. Since $a_3+a_4+a_5 = 0$, $a_1+a_2-1 = 0$ and $a_6 = -0.74$, there is no fixed point in map (11). Therefore, this chaotic attractor is hidden.

By coupling linear augmentation to the second equation of map (11), we obtain the following augmented map,

$$\begin{cases} x_{k+1} = y_k, \\ y_{k+1} = x_k + 0.51x_k^2 + y_k^2 - 1.51x_k y_k - 0.74 + \varepsilon u_k, \\ u_{k+1} = \delta u_k - \varepsilon(y_k - b). \end{cases} \tag{12}$$

Since map (12) is a three-dimensional map, it is difficult to distinguish between hidden and self-excited attractors by observing their basins of attraction. The usual random bifurcation diagrams can show the hidden and self-excited attractors if the initial points are chosen randomly as many as possible. The procedure to draw these bifurcation diagrams can be described as follows: (1) To take as many as possible initial points randomly for the initial branching parameter; (2) To plot the solutions of each initial point once it converges to an attractor; (3) To increase or decrease the branching parameter, and repeat the previous steps. However, by using this method, we cannot distinguish between hidden and self-excited attractors. So, in the present work, a new class of random bifurcation diagram is constructed to display the self-excited attractors by using the sampling method [Dudkowski *et al.*, 2016b; Brzeski & Perlikowski, 2019; Faghani *et al.*, 2020]. The new procedure can be described as follows: (1) To obtain the fixed points of map (11) by solving Eq. (8) for the initial branching parameter; (2) To take as many as possible initial points from the small neighbours of the fixed points randomly if they exist; (3) To plot the solutions of each initial point once it converges to an attractor, which is self-excited; (4) To increase or decrease the branching parameter, and repeat the previous steps. Next, we will demonstrate the evolution of self-excited attractors of map (11) by presenting their new bifurcation diagram. By comparing the results obtained from the traditional and the new random bifurcation diagrams, we can easily identify the differences between the hidden and self-excited attractors of map (12) defined by Definition 2.1.

Bifurcation diagram of the augmented map (12) calculated for $\delta = 0.5$ and $b = 0.5$ by using $\varepsilon$ as the branching parameter is shown in Fig. 1(a), where the random initial values were taken from the small neighbour ($< 0.001$) of the fixed point, and the self-excited attractors and stable fixed points are denoted

by SA and SFP, respectively. Figs. 1(b) and (c) present the bifurcation and Lyapunov exponent diagrams of the augment map (12) with respect to $\varepsilon$, where stable solutions (excluding the stable fixed point), stable fixed points and unstable fixed points (UFP) are marked by black, red and blue dots, respectively. The regions that have no attractors and hidden attractors are marked as NA and HA, respectively.

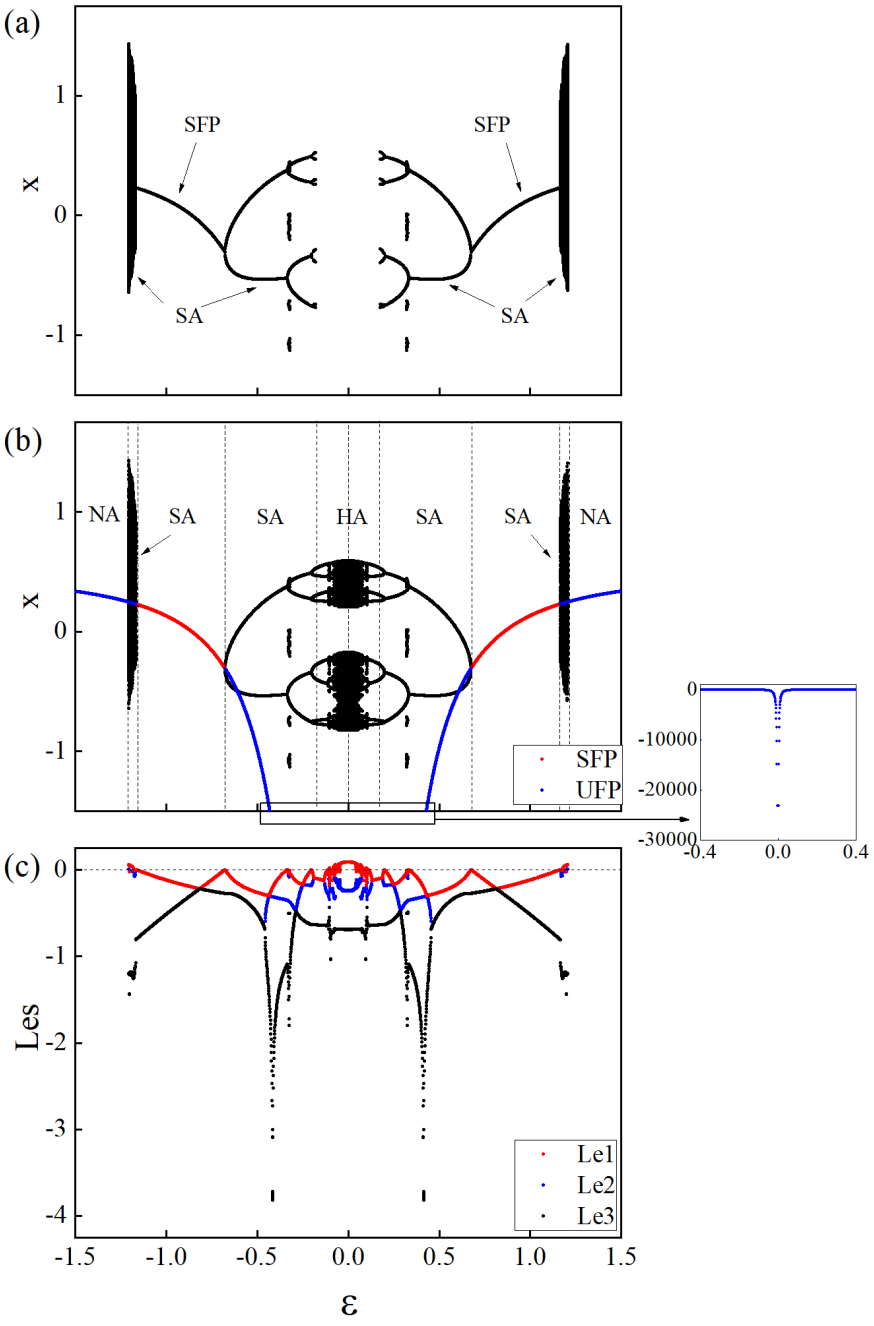


Fig. 1. (Colour online) (a) Bifurcation diagram of the augmented map (12) calculated for $\delta = 0.5$ and $b = 0.5$ by using $\varepsilon$ as the branching parameter, and random initial values taken from the small neighbour ($< 0.001$) of the fixed point. (b) Bifurcation and (c) Lyapunov exponent diagrams of the augmented map (12) calculated for $\delta = 0.5$ and $b = 0.5$ by using $\varepsilon$ as the branching parameter and random initial values taken from $x_k, y_k, u_k \in [-5, 5]$. Stable solutions (excluding the stable fixed point), stable fixed points (SFP) and unstable fixed points (UFP) are marked by black, red and blue dots, respectively. The regions that have no attractors (NA), self-excited attractors (SA) and hidden attractors (HA) are divided by dashed lines. The largest Lyapunov exponent (Le1), the second largest Lyapunov exponent (Le2) and the smallest Lyapunov exponent (Le3) are denoted by red, blue and black dots, respectively.

Phase portraits of the augmented map (12) on the $x-y$ plane calculated for $\delta = 0.5$, $b = 0.5$, and different $\varepsilon$ are presented in Fig. 2, where different attractors denoted by red, blue and black dots were obtained by using appropriate initial values. If $\varepsilon = 0$, there is no coupling between the nonlinear and the linear maps. So the state $(x, y)$ of the augmented map (12) has a single chaotic attractor which is the same as the attractor of the two-dimensional map (11) as shown in Fig. 2(a). Since there is no fixed point, this chaotic attractor is hidden. As can be seen from Fig. 1, as $\varepsilon$ increases from 0, there exists an unstable fixed point. If $\varepsilon$ is small, $(a_1 + a_2 - 1 - \frac{\varepsilon^2}{1-\delta})$ is very tiny, and the values of the unstable fixed points are large negative as shown in the additional window of Fig. 1(b). As $\varepsilon$ increases, a reverse period-doubling cascade was encountered leading the chaotic attractor to a period-2 orbit. Figs. 2(b)-(c) present the phase-portraits of some periodic orbits. According to Fig. 1(a), if $\varepsilon$ is small, the fixed point cannot be used for locating attractors, so these attractors can be considered as hidden [Jafari & Sprott, 2013]. As $\varepsilon$ increases, these attractors become self-excited, and a small regime of multi-stability was observed. Based on Fig. 2(d), our numerical simulation indicates that a period-12 and a period-2 orbits coexist, and both of them are self-excited. With the increase of $\varepsilon$, the augmented map (12) undergoes a reverse period-doubling bifurcation at $\varepsilon = 0.68$, and the period-2 orbit shown in Fig. 2(e) bifurcates into a stable fixed point as depicted in Fig. 2(f). At $\varepsilon = 1.17$, the map encounters a Neimark-Sacker bifurcation (where $\lambda_1 \approx -0.4435$, $\lambda_{2,3} \approx 0.5278 \pm 0.8499j$, and $|\lambda_{2,3}| \approx 1$), and the stable fixed point bifurcates into a quasi-periodic attractor forming a circle in three dimensional view, as presented in Fig. 2(g). Then the quasi-periodic attractor bifurcates into a chaotic attractor, as shown in Figs. 2(h) and (i), and disappears completely at $\varepsilon = 1.2$. As the bifurcation of the augmented map (12) is symmetric along $\varepsilon = 0$, the bifurcation for which $\varepsilon$ decreases from 0 will not be studied again here.

For the second example of NFI, we choose $a_1 = 1$, $a_2 = a_3 = 0$, $a_4 = 0.38$, $a_5 = -0.38$, and $a_6 = -1.60$, and the equations of the map ($\text{NFI}_f$ in [Jiang *et al.*, 2016a]) can be written as

$$\begin{cases} x_{k+1} = y_k, \\ y_{k+1} = x_k + 0.38y_k^2 - 0.38x_k y_k - 1.6. \end{cases} \tag{13}$$

According to [Jiang *et al.*, 2016a], map (13) has a period-2 orbit and a single chaotic attractor. Since $a_3 + a_4 + a_5 = 0$, $a_1 + a_2 - 1 = 0$ and $a_6 = -1.6$, there is no fixed point in the map, so the period-2 orbit and the chaotic attractor are all hidden.

By coupling a linear augmentation to map (13), we can obtain the following augmented map,

$$\begin{cases} x_{k+1} = y_k, \\ y_{k+1} = x_k + 0.38y_k^2 - 0.38x_k y_k - 1.6 + \varepsilon u_k, \\ u_{k+1} = \delta u_k - \varepsilon(y_k - b). \end{cases} \tag{14}$$

Bifurcation diagram of the augmented map (14) with respect to $\varepsilon$ calculated using $\delta = 0.5$, $b = 0.5$, and the random initial values taken from the small neighbour ($< 0.001$) of the fixed point (if exists) is presented in Fig. 3(a). Bifurcation and Lyapunov exponent diagrams of the map with respect to $\varepsilon$ calculated by using the random initial values taken from $x_k, y_k, u_k \in [-5, 5]$ are shown in Figs. 3(b) and (c), respectively.

Phase portraits of the augmented map (14) on the $x-y$ plane calculated for $\delta = 0.5$, $b = 0.5$, and different $\varepsilon$ are presented in Fig. 4, where different attractors denoted by red, blue and black dots were obtained by using appropriate initial values. When $\varepsilon = 0$, there is no coupling between the nonlinear and the linear maps, so the state $(x, y)$ of the augmented map (14) displays a period-2 orbit and a single chaotic attractor as shown in Fig. 4(a). According to Definition 2.1, both the period-2 orbit and the chaotic attractor are hidden. It can be seen from Fig. 3(b) that as $\varepsilon$ increases from 0, a small window of unstable fixed points was observed. If $\varepsilon$ is small, $(a_1 + a_2 - 1 - \frac{\varepsilon^2}{1-\delta})$ is very tiny, and the values of the unstable fixed points are large negative as presented in the additional window of Fig. 3(b). Figs. 4(b)-(d) demonstrate the evolution of the unstable fixed points after encountering a reverse period-doubling bifurcation cascade which leads the chaotic attractor to periodic orbits. As can be seen from Fig. 3(a), when $\varepsilon$ is small, the fixed point cannot be used for locating attractors, so the attractors of the augmented map (14) are hidden. In Fig. 4(c), the coexistence of the multiple hidden attractors, a period-36 orbit, a period-6 orbit, and a period-2 orbit, is presented. As $\varepsilon$ increases, these attractors become self-excited. Self-excited attractors were also recorded in Fig. 4(e), where a period-10 and a period-2 orbits coexist. At

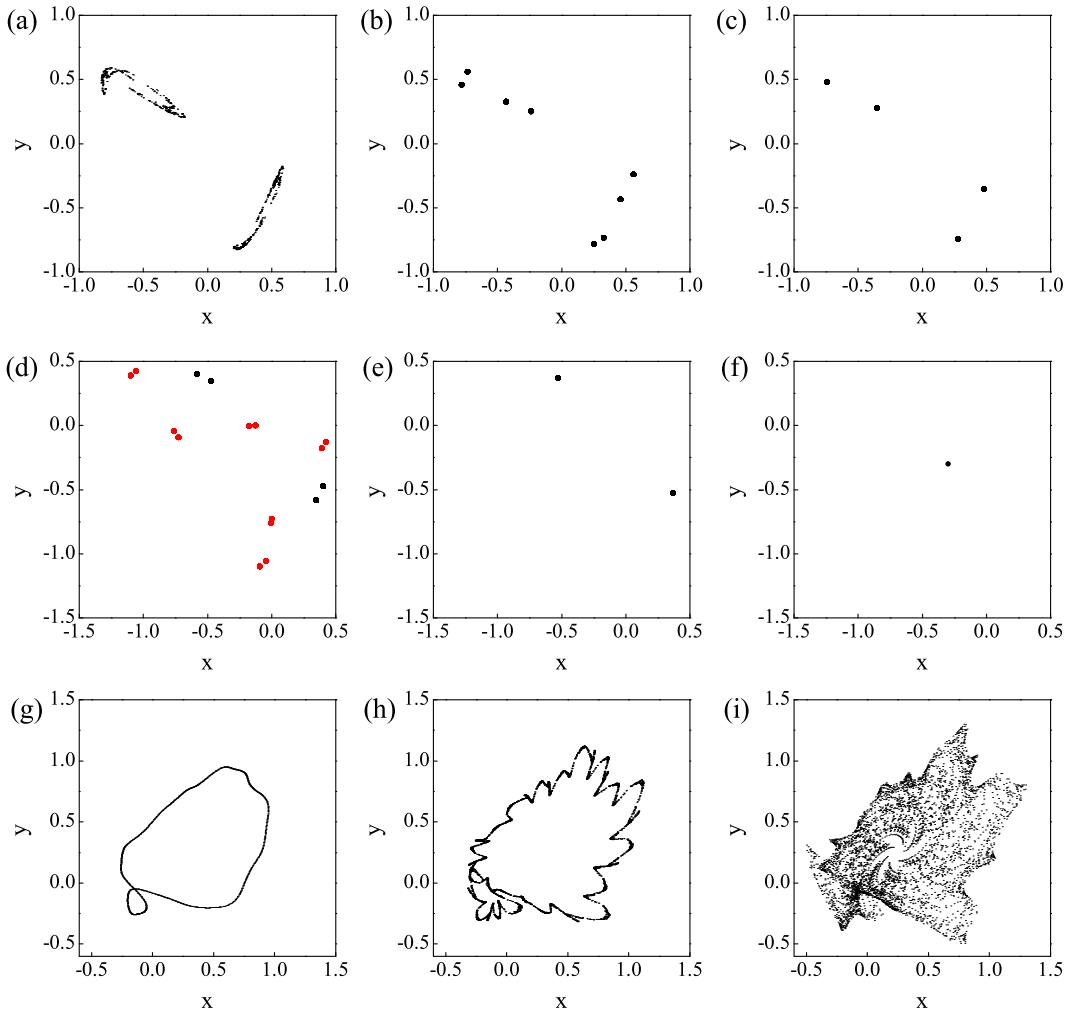


Fig. 2. (Colour online) Phase portraits of the augmented map (12) calculated for $\delta = 0.5$, $b = 0.5$, (a) $\varepsilon = 0$ (chaos) (b) $\varepsilon = 0.12$ (period-8 orbit), (c) $\varepsilon = 0.22$ (period-4 orbit), (d) $\varepsilon = 0.325$ (period-12 and period-4 orbits), (e) $\varepsilon = 0.34$ (period-2 orbit), (f) $\varepsilon = 0.68$ (stable fixed point), (g) $\varepsilon = 1.168$ (quasi-periodic orbit), (h) $\varepsilon = 1.18$ (chaos), and (i) $\varepsilon = 1.19$ (chaos) on the $x - y$ plane. Different attractors denoted by red, blue and black dots were obtained by using appropriate initial values.

$\varepsilon = 0.84$, the self-excited period-2 orbit bifurcates into a stable fixed point through a reverse period-doubling bifurcation as demonstrated in Fig. 4(f). At $\varepsilon = 1.23$, the map undergoes a Neimark-Sacker bifurcation (where $\lambda_1 \approx -0.5053$, $\lambda_{2,3} \approx 0.4973 \pm 0.8677j$, and $|\lambda_{2,3}| \approx 1$), and the stable fixed point bifurcates into a quasi-periodic attractor forming a circle as shown in Fig. 4(g). Then this quasi-periodic attractor becomes a chaotic attractor before a high-periodic orbit is encountered, which disappears completely at $\varepsilon = 1.273$. Again, as the bifurcation structure is symmetric along $\varepsilon = 0$, the bifurcation when $\varepsilon$ decreases will not be studied here.

### 3.2. *No Fixed Point II*

According to the study in [Jiang *et al.*, 2016a], if $a_3 + a_4 + a_5 \neq 0$ and $\Delta < 0$, Eq. (5) has no solution, and map (3) has no fixed point. Again, if there exists an attractor, it must be hidden since the basin of attraction of this attractor does not contain any fixed point. Since $a_3 + a_4 + a_5 \neq 0$, we can choose $\varepsilon$, $\delta$ and $b$ such that $\bar{\Delta} \geq 0$, then Eq. (5) has real solutions. Thus, the augmented map (6) has fixed points. To demonstrate this, we choose $a_1 = 0.6$, $a_2 = a_3 = 0$, $a_4 = 0.49$, $a_5 = -1$, and $a_6 = -1.46$, and the equations

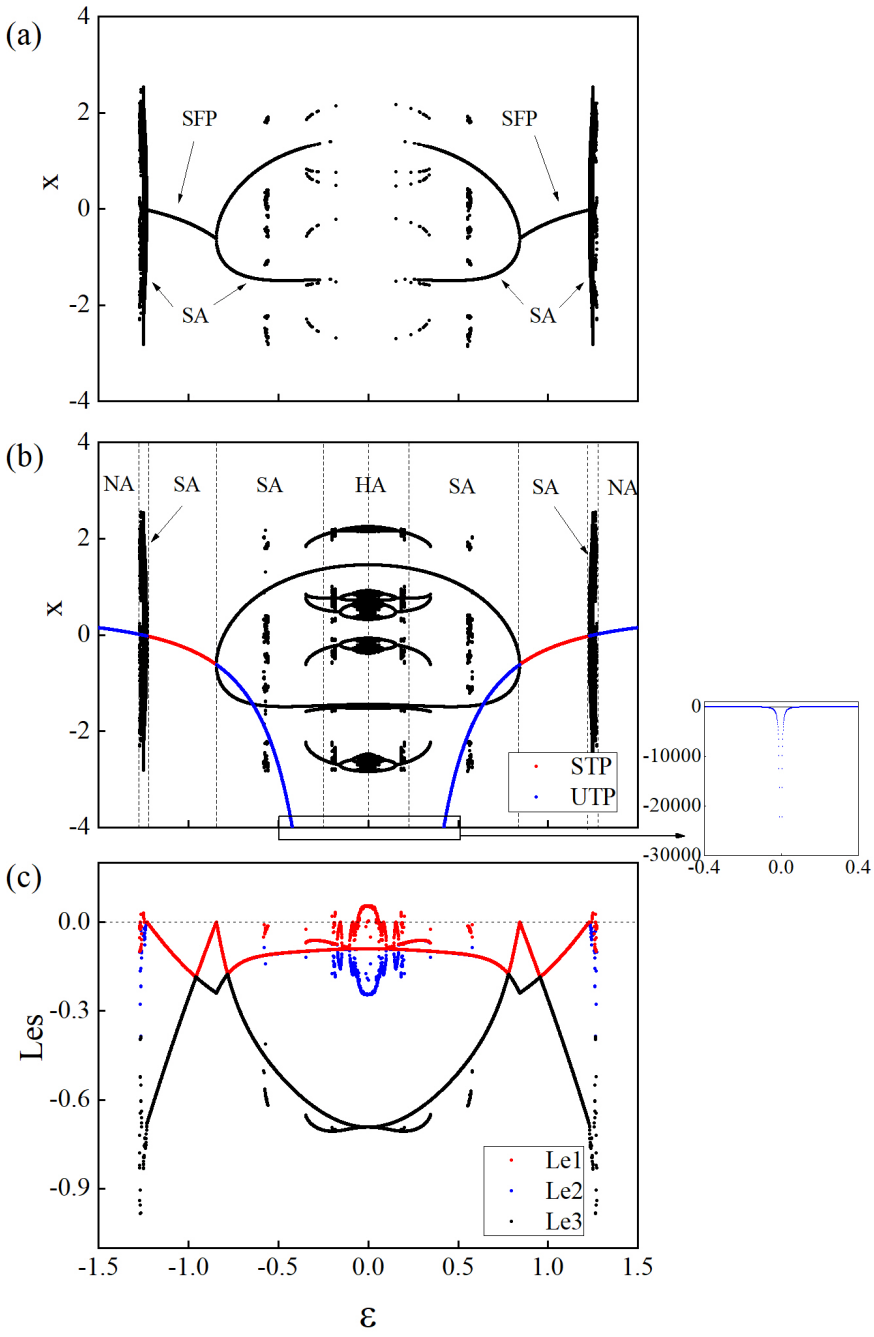


Fig. 3. (Colour online) (a) Bifurcation diagram of the augmented map (14) calculated for $\delta = 0.5$ and $b = 0.5$ with respect to $\varepsilon$ by using random initial values taken from the small neighbour ($< 0.001$) of the fixed point. (b) Bifurcation and (c) Lyapunov exponent diagrams of the map calculated for $\delta = 0.5$ and $b = 0.5$ by using $\varepsilon$ as the branching parameter and random initial values taken from $x_k, y_k, u_k \in [-5, 5]$. Stable solutions excluding stable fixed point, stable fixed points (SFP) and unstable fixed points (UFP) are marked by black, red and blue dots, respectively. The regions that have no attractors (NA), self-excited attractors (SA) and hidden attractors (HA) are divided by dashed lines. The largest Lyapunov exponent (Le1), the second largest Lyapunov exponent (Le2) and the smallest Lyapunov exponent (Le3) are denoted by red, blue and black dots, respectively.

of the map (NFII$_e$ in [Jiang *et al.*, 2016a]) can be written as

$$\begin{cases} x_{k+1} = y_k, \\ y_{k+1} = 0.6x_k + 0.49y_k^2 - x_k y_k - 1.46. \end{cases} \tag{15}$$

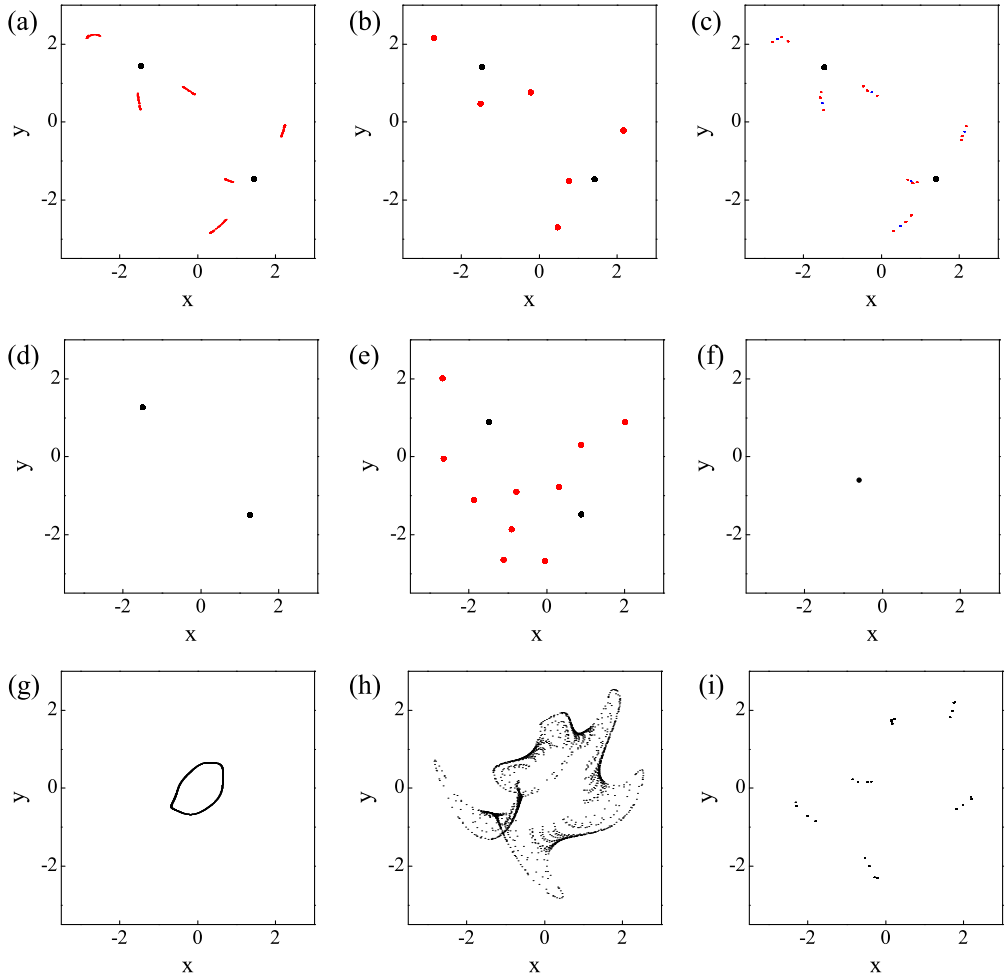


Fig. 4. (Colour online) Phase portraits of the augmented map (14) calculated for $\delta = 0.5$, $b = 0.5$, (a) $\varepsilon = 0$ (chaos and periodic-2 orbit), (b) $\varepsilon = 0.16$ (period-6 and period-2 orbits), (c) $\varepsilon = 0.19$ (period-36, period-6 and period-2 orbits), (d) $\varepsilon = 0.35$ (period-2 orbit), (e) $\varepsilon = 0.58$ (period-10 and period-2 orbits), (f) $\varepsilon = 0.85$ (stable fixed point), (g) $\varepsilon = 1.232$ (quasi-periodic orbit), (h) $\varepsilon = 1.25$ (chaos), and (i) $\varepsilon = 1.272$ (period-24 orbit) on the $x - y$ plane. Different attractors denoted by red, blue and black dots were obtained by using appropriate initial values.

Since $a_3 + a_4 + a_5 = -0.51$ and $\Delta = -2.8184$, there is no fixed point, and the map has a chaotic attractor, so this chaotic attractor is hidden.

By coupling the linear augmentation to the second equation of map (15), the following augmented map can be obtained,

$$\begin{cases} x_{k+1} = y_k, \\ y_{k+1} = 0.6x_k + 0.49y_k^2 - x_k y_k - 1.46 + \varepsilon u_k, \\ u_{k+1} = \delta u_k - \varepsilon(y_k - b). \end{cases} \tag{16}$$

To show the self-excited attractors of the augmented map (16), we repeated the same bifurcation analysis and bifurcation and Lyapunov exponent diagrams in NFI for map (16) with respect to $\varepsilon$, and presented them in Fig. 5. Once $\varepsilon = 0$, there is no coupling between the nonlinear and the linear maps. So the state $(x, y)$ of the augmented map (16) has a single chaotic attractor which is the same as the attractor of the two-dimensional map (15), as demonstrated in Fig. 6(a). As can be seen from Fig. 5, as $\varepsilon$ increases from 0, there is a reverse period-doubling bifurcation cascade leading the chaotic attractor to the period-$2n$ orbits (where $n = 1, 2, \cdots$), which are presented in Figs. 6(b)-(d). It should be noted that in the regions that no fixed point was found, their attractors are all hidden. With the increase of $\varepsilon$, $\bar{\Delta}$ is changed from zero to positive, and there exists one unstable fixed point (UTP) and two unstable fixed points (UFP)

accordingly. From Fig. 5(a), we can observe that the period-2 orbits are changed from hidden to self-excited. As $\varepsilon$ increases further, a reverse period-doubling bifurcation of the fixed points occurs at $\varepsilon = 0.76$, and the unstable fixed point is converted to a stable fixed point (SFP), as presented in Fig. 6(e). At $\varepsilon = 1.172$, the augmented map (16) undergoes a Neimark-Sacker bifurcation (where $\lambda_1 \approx -0.3138$, $\lambda_{2,3} \approx 0.4072 \pm 0.9136j$, and $|\lambda_{2,3}| \approx 1$), and the stable fixed point bifurcates into a quasi-periodic attractor which forms a circle (see Fig. 6(f)). Thereafter, tiny regimes of the high-periodic orbits and the chaotic attractors are observed, which are depicted in Figs. 6(g)-(i). As the bifurcation of the augmented map (16) is symmetric along $\varepsilon = 0$, the study of the bifurcation phenomenon when $\varepsilon$ decreases from 0 is omitted here.

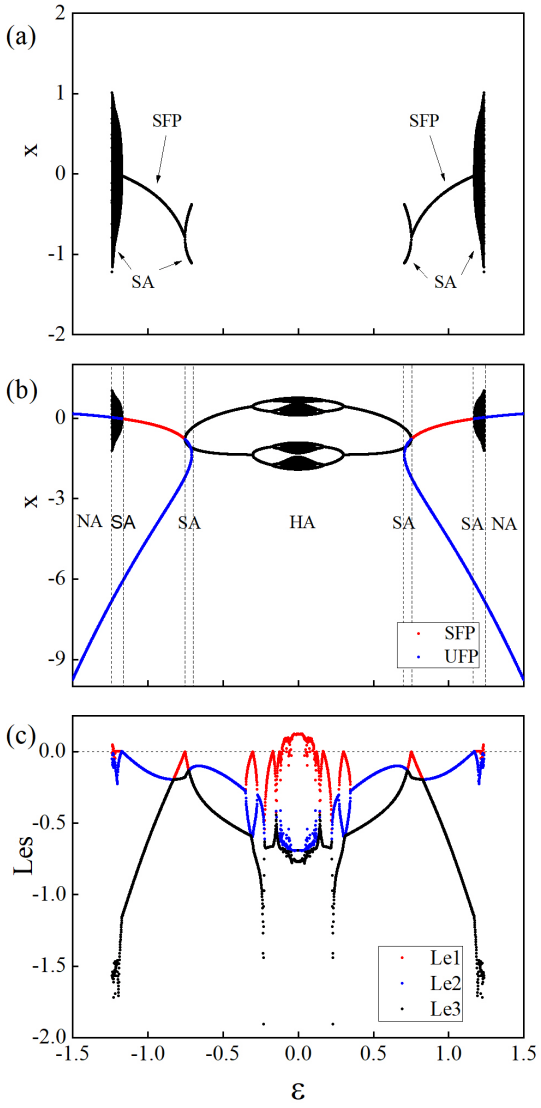


Fig. 5. (Colour online) (a) Bifurcation diagram of the augmented map (16) with respect to $\varepsilon \in [-1.5, 1.5]$, calculated for $\delta = 0.5$, $b = 0.5$, and initial values randomly taken from the small neighbour ($< 0.001$) of the fixed points. (b) Bifurcation and (c) Lyapunov exponent diagrams of the augmented map (16) with respect to $\varepsilon \in [-1.5, 1.5]$, calculated for $\delta = 0.5$, $b = 0.5$, and initial values randomly taken from $x_k, y_k, u_k \in [-5, 5]$. Stable solutions excluding the stable fixed point are denoted by black dots, stable fixed points (SFP) and unstable fixed points (UFP) are marked by red and blue dots, respectively. The regions that have no attractors (NA), self-excited attractors (SA), and hidden attractors (HA) are divided by dashed lines. The largest Lyapunov exponent (Le1), the second largest Lyapunov exponent (Le2), and the smallest Lyapunov exponent (Le3) are indicated by red, blue and black dots, respectively.

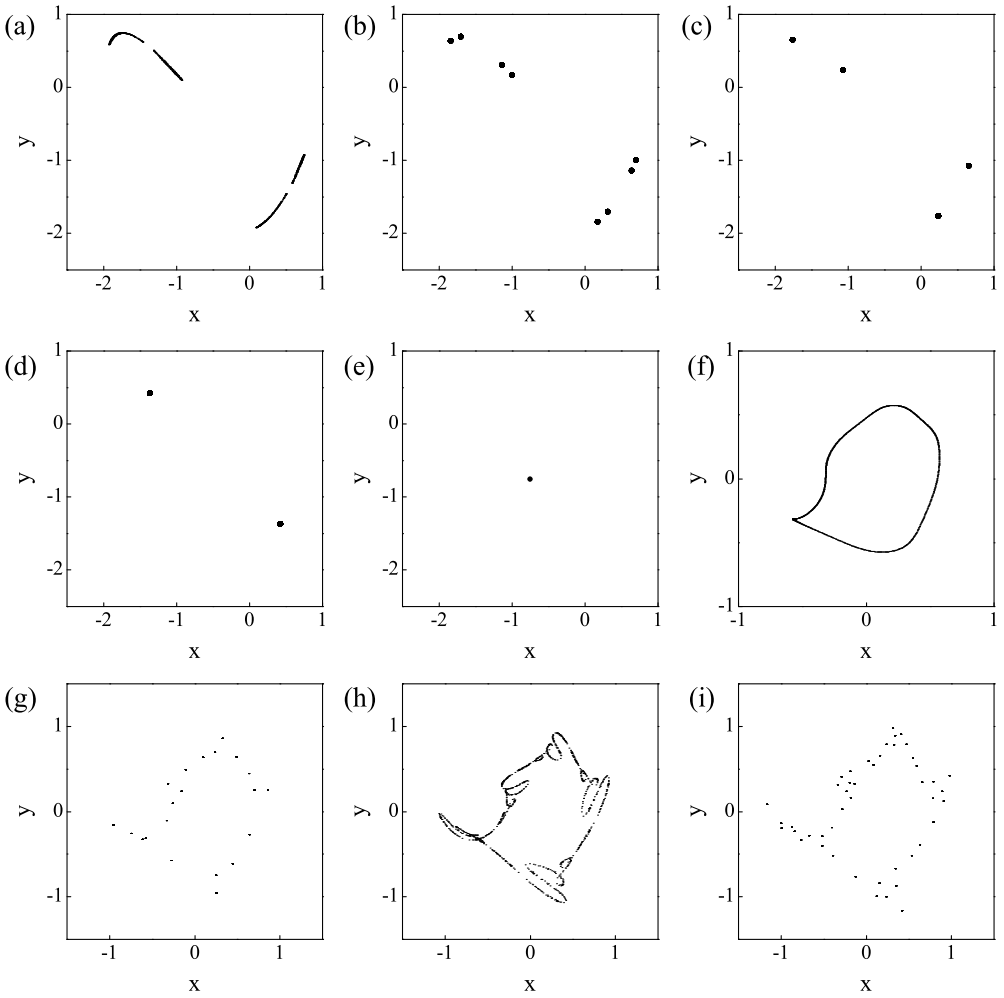


Fig. 6. Phase portraits of the augmented map (16) calculated for $\delta = 0.5$, $b = 0.5$, (a) $\varepsilon = 0$ (chaos) (b) $\varepsilon = 0.13$ (period-8 orbit), (c) $\varepsilon = 0.17$ (period-4 orbit), (d) $\varepsilon = 0.31$ (period-2 orbit), (e) $\varepsilon = 0.76$ (stable fixed point), (f) $\varepsilon = 1.19$ (quasi-periodic orbit), (g) $\varepsilon = 1.225$ (period-21 orbit), (h) $\varepsilon = 1.23$ (chaos), and (i) $\varepsilon = 1.225$ (period-46 orbit) on the $x - y$ plane.

## 4. Controlling two-dimensional maps with one stable fixed point via linear augmentation

When $a_3 + a_4 + a_5 = 0$ and $a_1 + a_2 - 1 \neq 0$, Eq. (5) has a single solution $y = -\frac{a_6}{a_1+a_2-1}$, and map (3) has a fixed point $(x^*, y^*)$, where $x^* = y^* = -\frac{a_6}{a_1+a_2-1}$. If the fixed point $(x^*, y^*)$ is stable, and the basins of attraction for the other attractors do not contain any fixed point, these attractors are hidden. Since $a_3 + a_4 + a_5 = 0$, we can choose $\varepsilon$, $\delta$, and $b$ such that $(a_1 + a_2 - 1 - \frac{\varepsilon^2}{1-\delta}) \neq 0$, and then Eq. (5) has a real solution. Thus, the augmented map (6) has a single fixed point. To demonstrate the control efficiency of the linear augmentation, we choose $a_1 = -0.84$, $a_2 = a_3 = 0$, $a_4 = 0.15$, $a_5 = -0.15$, and $a_6 = -5.85$, and the equations of the map ($\mathrm{SFI}_b$ in [Jiang *et al.*, 2016a]) can be written as

$$\begin{cases} x_{k+1} = y_k, \\ y_{k+1} = -0.84x_k + 0.15y_k^2 - 0.15x_k y_k - 5.85. \end{cases} \tag{17}$$

Since $a_3 + a_4 + a_5 = 0$ and $a_1 + a_2 - 1 \neq 0$, map (17) has a single stable fixed point. According to [Jiang *et al.*, 2016a], there is also a coexisting chaotic attractor. By coupling the linear augmentation, map (17)

can be rewritten as

$$\begin{cases} x_{k+1} = y_k, \\ y_{k+1} = -0.84x_k + 0.15y_k^2 - 0.15x_k y_k - 5.85 + \varepsilon u_k, \\ u_{k+1} = \delta u_k - \varepsilon(y_k - b). \end{cases} \tag{18}$$

Fig. 7(a) presents the self-excited attractors of the augmented map (18) by randomly taking the initial values from the small neighbour ($< 0.001$) of the fixed points. Figs. 7(b) and (c) show the bifurcation and the Lyapunov exponent diagrams of the augment map (18) with respect to $\varepsilon$ by randomly taking the initial values from $x_k, y_k, u_k \in [-5, 5]$, respectively. In Figs. 7(b) and (c), stable solutions (except the stable fixed points) are denoted by black dots, stable fixed points (SFP) and unstable fixed points (UFP) are marked by red and blue dots, respectively. The regions that have no attractors (NA), self-excited attractors (SA), and hidden attractors (HA) are divided by dashed lines.

When $\varepsilon = 0$, there is no coupling for the nonlinear map and the linear map. So the state $(x, y)$ of the augmented map displays a hidden chaotic attractor and a stable fixed point, which are the same as the attractors of the two-dimensional map (17), as shown in Fig. 8(a). It can be seen from Fig. 7, as $\varepsilon$ increases from 0, there is a reverse period-doubling bifurcation cascade leading the chaotic attractor to the period-$3n$ orbits (where $n = 1, 2, \cdots$). The phase-portraits of the period-12, the period-6 and the period-3 orbits recorded in this cascade are presented in Figs. 8(b)-(d). In particular, Fig. 8(b) displays the coexistence of a period-18 orbit, a period-12 orbit and a stable fixed point at $\varepsilon = 0.048$, which are all hidden except the stable fixed point, since the augmented map (18) has a single stable fixed point. With the increase of $\varepsilon$, the period-3 orbit ceases to exist at $\varepsilon = 0.221$, and only the stable fixed point is left, as demonstrated in Fig. 8(e). As $\varepsilon$ increases further, the augmented map (18) undergoes a Neimark-Sacker bifurcation at $\varepsilon = 0.742$ (where $\lambda_1 \approx 0.2848$, $\lambda_{2,3} \approx -0.0276 \pm 0.9997j$, and $|\lambda_{2,3}| \approx 1$), and the stable fixed point loses its stability bifurcating into a quasi-periodic attractor which forms a circle (see Fig. 8(f)), and disappears completely at $\varepsilon = 0.752$. Based on Fig. 7(a), we know that this quasi-periodic attractor and the chaotic attractors are all self-excited. As the bifurcation structure is symmetric along $\varepsilon = 0$, the bifurcation of the map when $\varepsilon$ decreases from 0 will also not be repeated here.

## 5. Conclusion

This paper presented the generalisation of linear augmentation which was used for controlling continuous dynamical systems to nonlinear maps, and investigated a class of two-dimensional maps containing hidden attractors by using the generalised linear augmentation. Four examples of the maps were considered, and the difference between these examples are as follows. For the first example, its hidden attractors were controlled to the self-excited periodic orbits, then to the period-2 orbits, and finally to the stable fixed points. For the second example, its hidden chaotic attractors were controlled to the self-excited periodic orbits before vanishing, and the coexisting period-2 orbits were controlled to the stable fixed points. The hidden attractors of the third example were controlled to the self-excited period-2 orbits, and then to the stable fixed points. For the last example, its hidden chaotic attractors were controlled to the hidden period-3 orbits before vanishing, and the coexisting stable fixed points bifurcated to the self-excited quasi-periodic attractors. According to the coupling strength of linear augmentation, hidden attractors of the map can be annihilated or converted to self-excited, and multi-stability of the map can be controlled to bistable or monostable. Furthermore, we also checked all the cases for the two-dimensional maps containing hidden attractors proposed in [Jiang *et al.*, 2016a], and their hidden dynamics and multi-stability can be controlled by choosing the parameters of the linear augmentation properly. Comparing with the other methods for controlling hidden dynamics or multi-stability in nonlinear maps, the proposed method can be easily implemented and does not require to change the parameters of the original map. It is general and effective to explore self-excited attractors and hidden attractors of nonlinear maps by constructing the traditional and new random bifurcation diagrams. The obtained results in the present work have broad applications, which can be applied to different disciplines including but not limited to economics, biology, and engineering. Our future work will focus on the investigation of linear augmentation for controlling high dimensional maps and the nonlinear maps with extreme multi-stability.

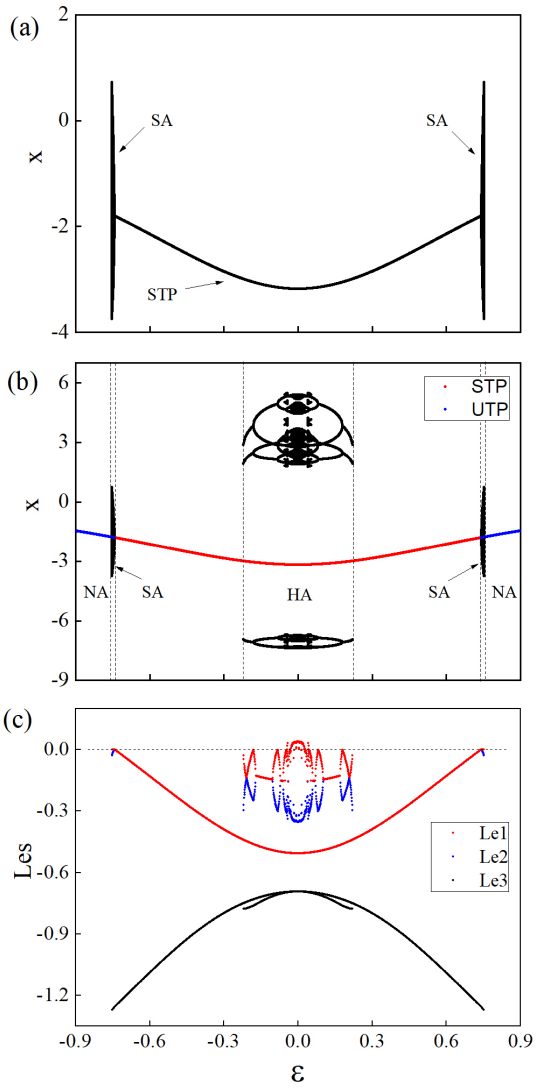


Fig. 7. (Colour online) (a) Bifurcation diagram of the augmented map (18) calculated for $\delta = 0.5$ and $b = 0.5$ by using $\varepsilon \in [-0.9, 0.9]$ as the branching parameter and random initial values taken from the small neighbour ($< 0.001$) of the fixed point. (b) Bifurcation and (c) Lyapunov exponent diagrams of the augmented map (18) with respect to $\varepsilon$ calculated for $\delta = 0.5$ and $b = 0.5$ and random initial values taken from $x_k, y_k, u_k \in [-5, 5]$. Stable solutions (excluding stable fixed points), stable fixed points (SFP) and unstable fixed points (UFP) are marked by black, red and blue dots, respectively. The regions that have no attractors (NA), self-excited attractors (SA) and hidden attractors (HA) are divided by dashed lines. The largest Lyapunov exponent (Le1), the second largest Lyapunov exponent (Le2) and the smallest Lyapunov exponent (Le3) are denoted by red, blue and black dots, respectively.

## Conflict of interests

The authors declare that there is no conflict of interests regarding the publication of this paper.

## Acknowledgements

The authors are grateful to the anonymous reviewers for their valuable comments and suggestions that have helped to improve the presentation of the paper. This work is partially supported by the National Natural Science Foundation of China (Grant Nos. 11672257, 11632008, 11772306 and 11972173), the Natural Science Foundation of Jiangsu Province of China (Grant No. BK20161314), the 5th 333 High-level Personnel Training Project of Jiangsu Province of China (Grant No. BRA2018324), and the Excellent Scientific and Technological Innovation Team of Jiangsu University.

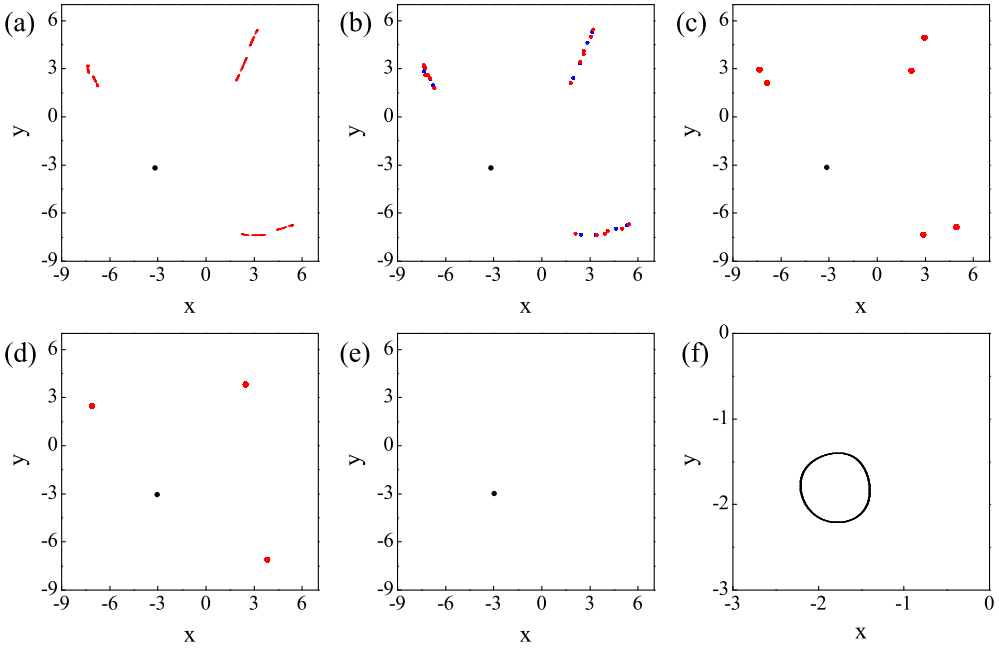


Fig. 8. (Colour online) Phase portraits of the augmented map (18) calculated for $\delta = 0.5$, $b = 0.5$, (a) $\varepsilon = 0$ (chaos and stable fixed point), (b) $\varepsilon = 0.048$ (period-18 orbit, period-12 orbit and stable fixed point), (c) $\varepsilon = 0.084$ (period-6 orbit and stable fixed point), (d) $\varepsilon = 0.181$ (period-3 orbit and stable fixed point), (e) $\varepsilon = 0.222$ (stable fixed point), and (f) $\varepsilon = 0.742$ (quasi-periodic orbit) on the $x - y$ plane. Different attractors denoted by red, blue and black dots were obtained by using appropriate initial values.

## References

Bao, B. C., Jiang, T., & Wang, G. Y. [2017] "Two memristor-based Chua's hyperchaotic circuit with plane equilibrium and its extreme multistability," *Nonlin. Dyn.*, **89**, 1157-1171.

Bao, B. C., Li, H. Z., Zhu, L., Zhang, X. & Chen, M. [2020] "Initial-switched boosting bifurcations in 2D hyperchaotic map," *Chaos*, **30**, 033107-1-14.

Barati, K., Jafari, S., Sprott, J. C. & Pham, V. [2016] "Simple chaotic flows with a curve of equilibria," *Int. J. Bifurcation and Chaos*, **26**, 1630034-1-8.

Brzeski, P. & Perlikowski, P. [2019] "Sample-based methods of analysis for multistable dynamical systems," *Arch. Computat. Methods Eng.*, 2019, **26**, 1515–1545.

Chen Y. & Yang Q. [2015] "A new Lorenz-type hyperchaotic system with a curve of equilibria," *Math. Comput. Simulat.*, **112**, 40–55.

Chen, E., Min, L. & Chen, G. [2017] "Discrete chaotic systems with one-line equilibria and their application to image encryption," *Int. J. Bifurcation and Chaos*, **27**, 1750046-1-17.

Dantsev, D. [2018] "A novel type of chaotic attractor for quadratic systems without equilibriums," *Int. J. Bifurcation and Chaos*, **28**, 1850001-1-7.

Dudkowski, D., Jafari, S., Kapitaniak, T., Kuznetsov N. V., Leonov, G. A. & Prasad, A. [2016a] "Hidden attractors in dynamical systems," *Phys. Rep.* **637**, 1–50.

Dudkowski, D., Prasad, A. & Kapitaniak, T. [2016b] "Perpetual points and periodic perpetual loci in maps," *Chaos*, **26**, 103103-1-9.

Faghani, Z., Nazarimehr, F., Jafari, S. & Sprott, J. C. [2020] "A new category of three-dimensional chaotic flows with identical eigenvalues," *Int. J. Bifurcation and Chaos*, **30**, 2050026-1-9.

Feng, Y. & Wei, Z. [2015] "Delayed feedback control and bifurcation analysis of the generalized Sprott B system with hidden attractors," *Eur. Phys. J. Special Topics*, **224**, 1619–1636.

Fonzin Fozin, T., Kengne, R., Kengne, J., Srinivasan, K., Souffo Tagueu, M. & Pelap, F. B. [2019] "Control of multistability in a self-excited memristive hyperchaotic oscillator," *Int. J. Bifurcation and Chaos*, **29**, 1950119-1-14.

Fonzin Fozin, T., Leutcho, G. D., Kouanou, A. T., Tanekou, G. B., Kengne, R., Kengne, J. & Pelap, F. B. [2019] "Multistability control of hysteresis and parallel bifurcation branches through a linear augmentation scheme," *Zeitschrift für Naturforschung A*, **75**, 11–21.

Fonzin Fozin, T., Megavarna Ezhilarasu, P., Njitacke Tabekoueng, Z., Leutcho, G. D., Kengne, J., Thamilmaran, K., Mezatio, A. B. & Pelap, F. B. [2019] "On the dynamics of a simplified canonical Chua's oscillator with smooth hyperbolic sine nonlinearity: hyperchaos, multistability and multistability control," *Chaos*, **29**, 113105-1-19.

Gotthans, T., Sprott, J. C. & Petržela, J. [2016] "Simple chaotic flow with circle and square equilibrium," *Int. J. Bifurcation and Chaos*, **26**, 1650137-1-8.

Jafari, S. & Sprott, J. C. [2013] "Simple chaotic flows with a line equilibrium," *Chaos Solit. Fract.*, **57**, 79–84.

Jafari, S., Sprott, J. C. & Golpayegani, S. [2013] "Elementary chaotic flows with no equilibria," *Phys. Lett. A* **377**, 699–702.

Jafari, S., Sprott, J. C. & Molaie, M. [2016a] "A simple chaotic flow with a plane of equilibria," *Int. J. Bifurcation and Chaos*, **26**, 1650098-1-6.

Jafari, S., Sprott, J. C., Pham, V. T., Volos, C. & Li, C.B. [2016b] "Simple chaotic 3D flows with surfaces of equilibria," *Nonlin. Dyn.*, **86**, 1349–1358.

Jafari, S., Pham, V. T., Moghtadaei, M. & Kingni, S. T. [2016c] "The relationship between chaotic maps and some chaotic systems with hidden attractors," *Int. J. Bifurcation and Chaos*, **26**, 1650211-1-8.

Jahanshahi, H., Shahriari-Kahkeshi, M., Alcaraz, R., Wang, X., Singh, V. P. & Pham, V. T. [2019] "Entropy analysis and neural network-based adaptive control of a non-equilibrium four-dimensional chaotic system with hidden attractors," *Entropy*, **21**, 156-1-15.

Jiang, H. B., Liu, Y., Wei, Z. & Zhang, L. P. [2016a] "Hidden chaotic attractors in a class of two-dimensional maps," *Nonlin. Dyn.*, **85**, 2719–2727.

Jiang, H. B., Liu, Y., Wei, Z. & Zhang, L. P. [2016b] "A new class of three-dimensional maps with hidden chaotic dynamics," *Int. J. Bifurcation and Chaos*, **26**, 1650206-1-13.

Jiang, H. B., Liu, Y., Wei, Z. & Zhang, L. P. [2019] "A new class of two-dimensional chaotic maps with closed curve fixed points," *Int. J. Bifurcation and Chaos*, **29**, 1950094-1-10.

Karnatak, R. [2015] "Linear augmentation for stabilizing stationary solutions: potential pitfalls and their application," *PLoS ONE* **10** e0142238-1-22.

Kuznetsov, Y.A. [1998] *Elements of Applied Bifurcation Theory*, 2nd edition (Springer-Verlag, NY).

Lai, Q., Nestor, T., Kengne, J. & Zhao, X. W. [2018] "Coexisting attractors and circuit implementation of a new 4D chaotic system with two equilibria," *Chaos Solit. Fract.*, **107**, 92–102.

Leonov, G. A., Kuznetsov, N. V. & Mokaev, T. N. [2015] "Hidden attractor and homoclinic orbit in Lorenz-like system describing convective fluid motion in rotating cavity," *Commun. Nonlinear Sci. Numer. Simul.*, **28**, 166–174.

Leonov, G. A. & Kuznetsov, N. V. [2013] "Hidden attractors in dynamical systems: from hidden oscillation in Hilbert-Kolmogorov, Aizerman and Kalman problems to hidden chaotic attractor in Chua circuits," *Int. J. Bifurcation and Chaos* **23**, 1330002-1-69.

Li, C. B., Sprott, J. C. & Thio, W. [2014a] "Bistability in a hyperchaotic system with a line equilibrium," *J. Exp. Theoretical Physics*, **118**, 494–500.

Li, Q., Hu, S., Tang, S. & Zeng, G. [2014b] "Hyperchaos and horseshoe in a 4D memristive system with a line of equilibria and its implementation," *Int. J. Circuit Theory Applications*, **42**, 1172–1188.

Liu, W. H., Sun, K. H. & He, S. B. [2017] "SF-SIMM high-dimensional hyperchaotic map and its performance analysis," *Nonlin. Dyn.*, **89**, 2521–2532.

Liu, Y. & Páez Chávez, J. [2017a] "Controlling coexisting attractors of an impacting system via linear augmentation," *Physica D* **348** 1–11.

Liu, Y. & Páez Chávez, J. [2017b] "Controlling multistability in a vibro-impact capsule system," *Nonlin. Dyn.*, **88**, 1289–1304.

Lin, W., Páez Chávez, J., Liu, Y., Yang, Y. & Kuang, Y. [2020] "Stick-slip suppression and speed tuning for a drill-string system via proportional-derivative control," *Appl. Math. Model.*, **82**, 487–502.

Liu, Y., Lin, W., Páez Chávez, J., & De Sa, R. [2019] "Torsional stick-slip vibrations and multistability in

drill-strings," *Appl. Math. Model.*, **76**, 545–557.
Lorenz, H. W. [1993] *Nonlinear Dynamical Economics and Chaotic Motion*, 2nd Ed. (Springer-Verlag, Berlin).
Mobayen, S. [2018] "Design of novel adaptive sliding mode controller for perturbed Chameleon hidden chaotic flow," *Nonlin. Dyn.*, **92**, 1539–1553.
Molate, M., Jafari, S., Sprott, J. C. & Golpayegani, S. [2013] "Simple chaotic flows with one stable equilibrium," *Int. J. Bifurcation and Chaos* **23**, 1350188-1-11.
Panahi, S., Sprott, J. C. & Jafari, S. [2018] "Two simplest quadratic chaotic maps without equilibrium," *Int. J. Bifurcation and Chaos*, **28**, 1850144-1-6.
Pham, V. T., Jafari, S. & Wang, X. [2016] "A chaotic system with different shapes of equilibria," *Int. J. Bifurcation and Chaos*, **26**, 1650069-1-5.
Pham, V. T., Volos, C. & Kapitaniak, T. [2017] *Systems with Hidden Attractors From Theory to Realization in Circuits* (Springer-Verlag, Berlin).
Sambas, A., Mamat, M., Arafa, A. A., Mahmoud, G. M., Mohamed, M. A. & Sanjaya, W.S. [2019] "A new chaotic system with line of equilibria: dynamics, passive control and circuit design," *Int. J. Electr. Comput. Eng.*, **9**, 2365–2376.
Sharma, P. R., Sharma, A., Shrimali, M. D. & Prasad, A. [2011] "Targeting fixed-point solutions in nonlinear oscillators through linear augmentation," *Phys. Rev. E*, **83**, 067201-1-4.
Sharma, P. R., Shrimali, M. D., Prasad, A. & Feudel, U. [2013] "Controlling bistability by linear augmentation," *Phys. Lett. A*, **377**, 2329–2332.
Sharma, P. R., Singh, A., Prasad, A. & Shrimali, M. D. [2014] "Controlling dynamical behavior of drive-response system through linear augmentation," *Eur. Phys. J. Special Topics*, **223**, 1531–1539.
Singh, J. P., Roy, B. K. & Jafari, S. [2018] "New family of 4-D hyperchaotic and chaotic systems with quadric surfaces of equilibria," *Chaos Solit. Fract.*, **106**, 243–257.
Tabekoueng Njitacke, Z., Sami Doubla, I., Kengne, J. & Cheukem, A. [2020] "Coexistence of firing patterns and its control in two neurons coupled through an asymmetric electrical synapse," *Chaos*, **30**, 023101-1-16.
Thounaojam, U. S. & Shrimali, M. D. [2018] "Phase-flip in relay oscillators via linear augmentation," *Chaos Solit. Fract.*, **107**, 5–12.
Vaidyanathan, S., Jafari, S. A. J. A. D., Pham, V. T., Azar, A. T. & Alsaadi, F. E. [2018] "A 4-D chaotic hyperjerk system with a hidden attractor, adaptive backstepping control and circuit design," *Arch. Control Sci.*, **28**, 239–254.
Wang, X. & Chen, G. [2012] "A chaotic system with only one stable equilibrium," *Commun. Nonlinear Sci. Numer. Simul.*, **17**, 1264-1272.
Wang, X. & Chen, G. [2013] "Constructing a chaotic system with any number of equilibria," *Nonlin. Dyn.*, **71**, 429–436.
Wang, Z., Sun, W., Wei, Z. & Zhang, S. [2015] "Dynamics and delayed feedback control for a 3D jerk system with hidden attractor," *Nonlin. Dyn.*, **82**, 577–588.
Wang, Z., Ma, J., Cang, S., Wang, Z. & Chen, Z. [2016] "Simplified hyper-chaotic systems generating multi-wing non-equilibrium attractors," *Optik*, **127**, 2424–2431.
Wang, X., Pham, V. T. & Volos, C. [2017] "Dynamics, circuit design, and synchronization of a new chaotic system with closed curve equilibrium," *Complexity*, **2017**, 7138971-1-9.
Wang, C. F. & Ding, Q. [2018] "A new two-dimensional map with hidden attractors," *Entropy*, **322**, 22-1-10.
Wei, Z. [2011] "Dynamical behaviors of a chaotic system with no equilibria," *Phys. Lett. A*, **376**, 102–108.
Wei, Z., Moroz, I. & Liu, A. [2014] "Degenerate Hopf bifurcations, hidden attractors, and control in the extended Sprott E system with only one stable equilibrium," *Turk. J. Math.*, **38**, 672–687.
Wei, Z. & Zhang, W. [2014] "Hidden hyperchaotic attractors in a modified Lorenz-Stenflo system with only one stable equilibrium," *Int. J. Bifurcation and Chaos* **24**, 1450127-1-14.
Wei, Z., Akgul, A., Kocamaz, U. E., Moroz, I. & Zhang, W. [2018] "Control, electronic circuit application and fractional-order analysis of hidden chaotic attractors in the self-exciting homopolar disc dynamo," *Chaos Solit. Fract.*, **111**, 157–168.

Zhang, S., Zeng, Y. C., Li, Z. J., Wang, M. J. & Xiong L. [2018] "Generating one to four-wing hidden attractors in a novel 4D no-equilibrium chaotic system with extreme multistability," *Chaos*, **28**, 013113-1-11.

Zhang, L. P., Liu, Y., Wei, Z., Jiang, H. B. & Bi, Q. S. [2020] "A novel class of two-dimensional chaotic maps with infinitely many coexisting attractors," *Chin. Phys. B*, **29**, 060501-1-6.

Zhou, P. & Yang, F. [2014] "Hyperchaos, chaos, and horseshoe in a 4D nonlinear system with an infinite number of equilibrium points," *Nonlin. Dyn.*, **76**, 473–480.